GPS Solutions (2019) 23:28
https://doi.org/10.1007/s10291-018-0813-z

ORIGINAL ARTICLE

1 Hz GPS satellites clock correction estimations to support high-rate dynamic PPP GPS applied on the Severn suspension bridge for deflection detection

Xu Tang[1] · Xingxing Li[2] · Gethin Wyn Roberts[3] · Craig Matthew Hancock[1] · Huib de Ligt[1] · Fei Guo[2]

Received: 14 March 2018 / Accepted: 14 November 2018
© Springer-Verlag GmbH Germany, part of Springer Nature 2019

Abstract
The use of GPS for deflection and vibration detection in structures requires a data rate of 1 Hz or higher. We investigate the advantages of utilizing high-rate satellite clocks in a dynamic PPP processing strategy specifically applied to the measurement of the deflections of bridges. A dataset consisting of 96 globally distributed stations was used for GPS satellite clocks estimates. The undifferenced float ambiguity (FAmb) and the Zenith Total Delay (ZTD) parameters were first estimated using PPP in static mode. The 1 Hz clock products of the GPS satellites were then successfully estimated by applying the FAmb and tropospheric delays as constraints to the carrier phase. The techniques are compared to 30-s and 300-s clock corrections obtained from the IGS, as well as double differenced solutions, through two experiments. The first experiment uses a rotating-arm apparatus, consisting of a portable rig located at the University of Nottingham Ningbo China, incorporating a 4 m long arm that rotates at a constant speed through the use of an electric motor. The 1-s GPS satellite clocks gave the most precise and stable PPP solution. The second experiment investigates the dynamic deflections of the Severn Bridge's suspension cables and towers, estimated using both the PPP, using our 1-s clock corrections as well as the IGS's 30-s and 300-s clock corrections, and the double differenced (DD) GPS data processing method. Correlation coefficient and standard deviation of the PPP solution and DD solution reflect the bridge's displacement waveform consistency and accuracy, respectively. Numerical analysis of the correlation coefficient and standard deviation of the time series, processed with different satellite clock intervals, implies that improvement can be achieved by applying the short interval satellites clock products that we propose. The strong agreement of the waveforms, calculated from the high-rate PPP, with the DD and the bridge load data, demonstrates that high-rate PPP is a viable alternative to the DD method for structural monitoring and an optimal option at times when DD is impossible due to the failure or inappropriateness of using a reference station.

Keywords Satellite clock correction · Bridge deflection monitoring · Precise point positioning · Real-time kinematic

Introduction

The use of GPS is a well-established method for measuring deformations and deflections of bridges (Ashkenazi and Roberts 1997; Roberts et al. 2014). With the introduction of more global navigation satellite systems, multi-GNSS is used for improving the precision of position estimations for structural movement detection (Msaewe et al. 2017). The vast majority of previous GPS bridge monitoring studies use DD GPS methods (Kaloop and Li 2009; Yi et al. 2013). DD GPS offers sub-centimeter accuracy measurements of 3D deflection of bridges and other large structures equipped with a GPS receiver. This sub-centimeter accuracy can be achieved since the DD method eliminates major GPS error sources over relatively short distances and the GPS satellites and receivers' clocks errors. DD GPS applications are limited in cases that require a long distance between a base station and a rover. Such examples include situations where the rover is isolated from land, such as on a very long sea-bridge, or situations where the base station moves in the same manner as the rover, such as in earthquake scenarios.

✉ Xu Tang
Xu.Tang@nottingham.edu.cn; Xu.Tang@hotmail.com

[1] University of Nottingham Ningbo China, 199 Taikang East Road, Ningbo 315100, Zhejiang, China

[2] Wuhan University, 129 Luoyu Road, Wuhan 430079, Hubei, China

[3] University of the Faroe Islands, Tórshavn, Faroe Islands

Published online: 09 January 2019

PPP delivers the required precision for bridge deflection monitoring after approximately half an hour of convergence time (Liu et al. 2017; Feng et al. 2013). PPP has been successfully applied to bridge suspension cables for deflection detection in the vertical component, but has been shown to be less able in extracting smaller displacements in the suspension cable in the longitudinal and lateral components (Tang and Li 2017a, b; Tang et al. 2017). Therefore, PPP is suitable for detecting large movements that occur over a short period but is less suitable for detecting small movements over longer periods (Moschas et al. 2014). PPP accuracy is degraded by the long-term unmodeled corrections, measurement noise or using IGS products improperly (Feng et al. 2013), for instance, processing high-rate sampled GPS observations using 300-s interval satellite clock product.

Satellite clocks and orbits are precisely modeled and are provided by many GNSS analysis centers from around the world. The IGS Analysis Center Coordinator (IGSACC) combines the clock products from centers using a weighted average and provides two types of final satellite clock products with 300-s and 30-s intervals between neighboring epochs. 30-s and 5-s interval clock products are also available from CODE (Center for Orbit Determination in Europe) for addressing high-frequency applications. The GPS sampling rate for bridge deformation applications is normally up to 20 Hz, allowing high structural vibration frequencies to be extracted. High-rate GPS clock corrections are required in order to be able to apply PPP in high-frequency oscillating applications. Bock et al. (2009) assessed the performance of high-rate satellite corrections for PPP precision improvement. The previous studies implied that low-rate sampling of GPS satellite clock corrections hampered the PPP positioning precision.

We present two experiments for assessing PPP performance using different interval satellites clocks products. The first uses a portable rotating-arm apparatus, located at the University of Nottingham Ningbo China (UNNC) campus. The dataset was processed using the PPP method with 30-s and 300-s interval satellite clock products from the IGSACC, and the 1-s clock products calculated for the purpose of this study. The second experiment incorporates our work on GPS data gathered on the Severn Suspension Bridge in the UK, again processing the data using the 1-s clock product and the 30-s and 300-s IGS clock products. The results of both experiments are compared to the DD results.

1 Hz satellite clock corrections estimation

This section describes how the 1 Hz satellite clock corrections are estimated using the GPS 1 Hz observations. In order to demonstrate how geometry affects the quality of satellite clock corrections, two GPS measurement datasets were collected. Two batches of 1 Hz satellite clock corrections were estimated using the UNNC standalone reference station and 96 globally distributed IGS stations. The standalone reference station observations were gathered at a rate of 1 Hz on the roof of the Sir Peter Mansfield Building (PMB) at UNNC, from GPS UTC time 04:00–08:00 on June 15, 2016. The 1 Hz sampling rate IGS observation files were obtained from the IGS global data center Crustal Dynamics Data Information Service (CDDIS), Greenbelt, Maryland, USA. The top panel of Fig. 1 shows that the UNNC station is located in a reasonably open sky environment. The bottom panel shows the distribution of the 96 IGS stations that were used to compute the satellite clock corrections. These globally distributed stations allow all the GPS satellites to be simultaneously tracked by multiple stations.

The receiver clock offsets at the UNNC reference station and those using all the 96 IGS stations are computed using the Standard Point Positioning (SPP) algorithm. The parameters of the ZTD, FAmb and positions of the IGS stations are then computed using static PPP with either 30-s or 300-s intervals between the neighboring epochs. Linear

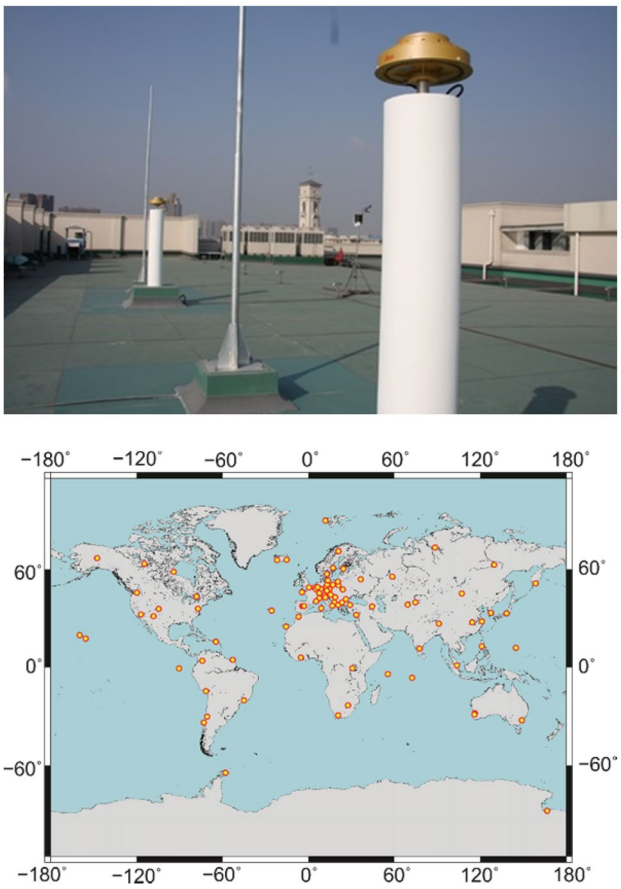


Fig. 1 Stable GNSS stations (top) on the roof of PMB at UNNC with a reasonably open sky environment and the distribution of the 96 IGS stations

interpolation is used to generate the 1-s interval ZTD, FAmb and position parameters. The 1 s interval ZTD, FAmb, position parameters, receiver clock offsets and ionosphere-free (IF) observation are then used to generate the 1 Hz satellite clock correction estimation.

FAmb and ZTD parameters estimation

The mapping function allows all troposphere delays in the "line-of-sight" of each satellite to be expressed in the zenith direction. With an assumption of n stations and m satellites, implementation of a mapping function reduces the number of unknown troposphere delay parameters from m to 1. The Niell mapping function (NMF) was used in this study (Niell 1996). The number of unknown parameters is $n \times (5 + m)$ at each epoch, which includes three position unknown parameters, one receiver clock offset, one unknown troposphere delay related parameter, as well as m unknown FAmb parameters at all stations. The IF measurement vector of the observation equation is,

$$\left[\boldsymbol{\varphi}_1, \ldots, \boldsymbol{\varphi}_i, \ \ldots, \boldsymbol{\varphi}_n\right]^T_{1\times(m_1+\cdots+m_i+\cdots+m_n)}, \ \{i = [1,n], \ i \in Z\}, \tag{1}$$

where $\boldsymbol{\varphi}_i$ is the ionosphere-free measurement row-vector which has m_i elements at the ith station at individual epoch. m is the number of unique satellites that are tracked by all n stations. $m_1 = \cdots = m_i = \cdots = m_n = m$, as long as all stations are located in a small region.

The state of the Extended Kalman Filter (EKF) in static PPP for estimating positions, troposphere delay parameters and satellites FAmbs at all stations is,

$$\left(\boldsymbol{\Upsilon}_1, \ldots, \boldsymbol{\Upsilon}_i, \ldots \boldsymbol{\Upsilon}_n, \boldsymbol{N}^1, \ldots, \boldsymbol{N}^j, \ldots, \boldsymbol{N}^m\right)^T_{1\times(5n+mn)}, \ \{i = [1,n], j = [1,m] \cap i,j \in Z\}, \tag{2}$$

where vector $\boldsymbol{\Upsilon}_i$ represents the ith station parameters $\left[x, y, z, \delta t, \delta_{\mathrm{ZTD}}\right]$, contains 3D position $\left[x, y, z\right]$, receiver clock offset δt, and zenith total delay δ_{ZTD}. $\boldsymbol{N}^j$ is a $1 \times n$ vector, represents the jth satellite's float carrier phase ambiguities at all satellites.

The EKF Jacobean-matrix $\boldsymbol{H}$ is designed as,

$$H = \left[\boldsymbol{\Gamma}, \boldsymbol{I}^1, \ldots, \boldsymbol{I}^j, \ldots, \boldsymbol{I}^m\right]_{(m_1+\cdots+m_i+\cdots+m_n)\times(5n+mn)}, \ \{j = [1,m], j \in Z\}, \tag{3}$$

where $\boldsymbol{\Gamma}$ is a diagonal matrix with the element $\Gamma_1, \ldots, \Gamma_i, \ldots, \Gamma_n$.

$$\Gamma = \begin{bmatrix} \Gamma_1 & \cdots & 0 & 0 \\ \vdots & \ddots & & \\ 0 & & \Gamma_i & \cdots \\ & & \vdots & \ddots \\ 0 & & 0 & \Gamma_n \end{bmatrix}_{(m_1+\cdots+m_i+\cdots+m_n)\times 5n}, \{i = [1,n], i \in Z\}. \tag{4}$$

In (4) Γ_i is a $m_i \times 5$ matrix, coefficient of $\boldsymbol{\Upsilon}_i$ at the ith station.

$$\boldsymbol{\Gamma}_i = \begin{bmatrix} \partial x_i^1/\rho_i^1 & \partial y_i^1/\rho_i^1 & \partial z_i^1/\rho_i^1 & 1 & M_i^1 \\ & \vdots & & \vdots & \\ \partial x_i^j/\rho_i^j & \partial y_i^j/\rho_i^j & \partial z_i^j/\rho_i^j & 1 & M_i^j \\ & \vdots & & \vdots & \\ \partial x_i^{m_i}/\rho_i^{m_i} & \partial y_i^{m_i}/\rho_i^{m_i} & \partial z_i^{m_i}/\rho_i^{m_i} & 1 & M_i^{m_i} \end{bmatrix}_{m_i\times 5}, \{i = [1,n], j = [1,m], i,j \in Z\}, \tag{5}$$

$\boldsymbol{I}^j$ is the coefficient matrix of the jth. satel FAmbs at all stations in (5). M_i^j is the jth satellite's zenith wet delay mapping function coefficient at the ith station. The matrix dimension is $\left(m_1 + \ldots + m_i + \cdots + m_n\right) \times n$. The row of $\boldsymbol{I}^j$. is sorted by the IF measurements at each station, the column of $\boldsymbol{I}^j$ is sorted by the stations.

$$\boldsymbol{I}^j = \begin{bmatrix} I_1^j & 0 & 0 & 0 & 0 \\ \vdots & \vdots & \vdots & \vdots & \vdots \\ 0 & 0 & I_i^j & 0 & 0 \\ \vdots & \vdots & \vdots & \vdots & \vdots \\ 0 & 0 & 0 & 0 & I_n^j \end{bmatrix}_{(m_1+\cdots+m_i+\cdots+m_n)\times n}, \ \{i = [1,n], j = [1,m] \cap i,j \in Z\}, \tag{6}$$

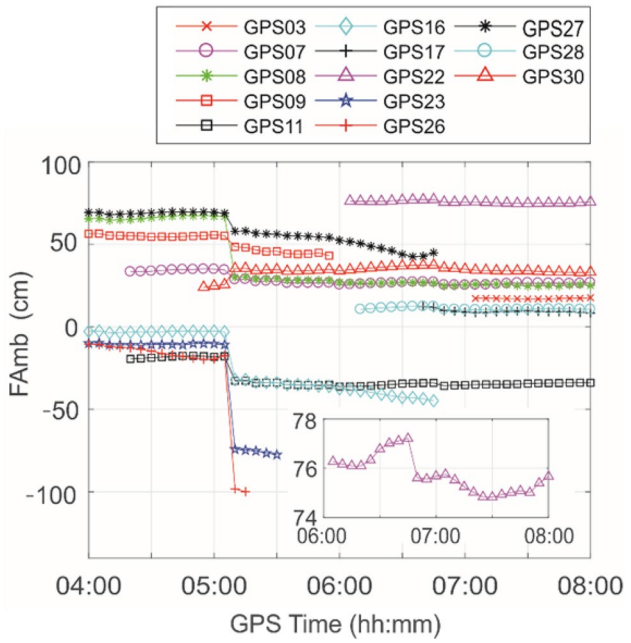


Fig. 2 GPS satellite carrier phase float ambiguities over 4 h, calculated using the UNNC GNSS reference station on the roof of PMB

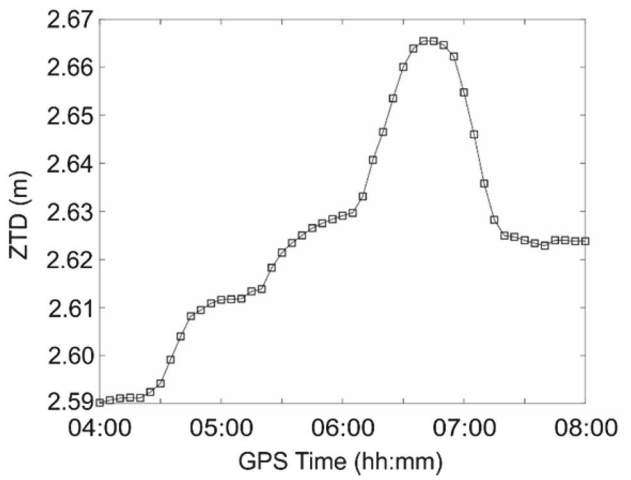


Fig. 3 Zenith Total Delay over 4 h, calculated from the dataset collected at the GNSS reference station on the roof of PMB at UNNC on June 15, 2016

column vector I_i^j in $\boldsymbol{I}^j$. is the coefficient the jth satellite's FAmb at the ith. station. There are m_i satellites tracked at this specified epoch. I_i^j has only one "1" and $m_i - 1$ "0".

Dataset from the UNNC station were processed for calculating the satellites' FAmbs and station ZTD every 300 s. There were 13 satellites tracked during the observation period. Figure 2 shows the stable FAmbs estimated by the static PPP model. The steps in the FAmbs time series between 5:00 and 5:20 are due to a data gathering gap. Most of the satellites' FAmbs are quite stable, although a few of them change gradually. The auxiliary Fig. 2 shows the FAmb calculated from measures to GPS PRN 22 between 6:00 and 8:00, indicating approximate 2 cm changes over the 2-h period. GPS PRN 27 FAmb are shown to be very stable before the signal is lost at about 5:10, but changes gradually after the signal is reacquired.

The tropospheric delay is a time variable, which is determined by the GNSS surveying point meteorological parameters. The hydrostatic delay can be precisely modeled with millimeter-level precision. The wet delay depends on the local weather. ZTD are estimated in this study. Figure 3 illustrates the estimated ZTD over the 4-h surveying period at UNNC. ZTD changes by up to 7.5 cm over the 4 h.

Both satellites' FAmbs and ZTD are very stable and change gradually. The high-rate of FAmb and ZTD corrections for satellite clock estimation can be achieved by using a linear interpolation algorithm. Continual observation is recommended for the stable and consistent precision of satellite clock correction estimation.

1-s interval GPS satellite clock correction estimation

With the estimates of FAmb, ZTD and position coordinate using static PPP, the GNSS satellite clock correction estimation equation can be written as,

$$\varphi_{\mathrm{IF},i}^j = \Delta T^j + \Delta T_i + \rho_i^j + M_i^{h,j} \cdot \delta_{\mathrm{ZHD},i} + M_i^{w,j} \cdot \delta_{\mathrm{ZWD},i} + N_i^j, \tag{7}$$

where φ_{IF} is the IF linear combination of carrier phase measurements, j denotes the jth satellite, and i denotes the ith station. ΔT^j. denotes the jth. GNSS clock correction, the estimation of which will be described in this section. ΔT_i is the ith station receiver clock offset, which is estimated by SPP. ρ_i^j denotes the receiver-satellite geometric range between the ith station receiver and the jth satellite. ρ is calculated using the satellite precise orbit products and receiver precise position derived by the static PPP. $M_i^{h,j}$ denotes the hydrostatic mapping function coefficient of satellite j at station i. $\delta_{\mathrm{ZHD},i}$ is computed using the empirical model. $M_i^{w,j}$ is the wet mapping coefficient of satellite j station $i\delta_{\mathrm{ZWD},i}$ is the zenith wet delay at ith station, which is estimated using static PPP. N_i^j denotes the jth satellite ambiguity, which is estimated using static PPP at the ith station GNSS receiver.

The satellite clock correction estimation. Equation in the matrix can be written as,

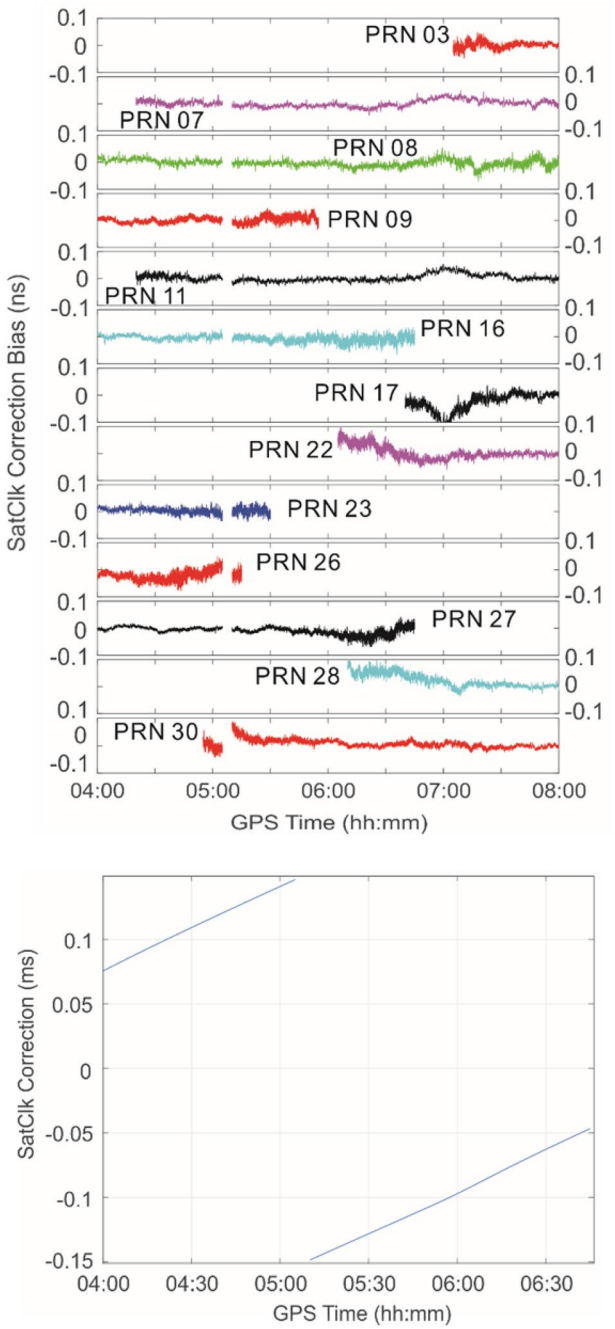


Fig. 4 GPS clock correction biases, corrections are estimated by the dataset, collected at the GNSS reference station on the roof of PMB at UNNC on June 15, 2016 (top). GPS PRN 16 clock correction, estimated by the dataset, collected at the GNSS reference station on the roof of PMB at UNNC on June 15, 2016 (bottom)

$$\begin{bmatrix} \boldsymbol{u}_1 \\ \vdots \\ \boldsymbol{u}_i \\ \vdots \\ \boldsymbol{u}_n \end{bmatrix}_{(m_1+\cdots+m_i+\cdots+m_n)\times 32} \cdot \begin{bmatrix} \Delta T^1 \\ \vdots \\ \Delta T^j \\ \vdots \\ \Delta T^{32} \end{bmatrix}_{32\times 1} = \begin{bmatrix} \boldsymbol{\varphi}_{1,IF} \\ \vdots \\ \boldsymbol{\varphi}_{i,IF} \\ \vdots \\ \boldsymbol{\varphi}_{n,IF} \end{bmatrix}_{(m_1+\cdots+m_i+\cdots+m_n)\times 1}, \tag{8}$$

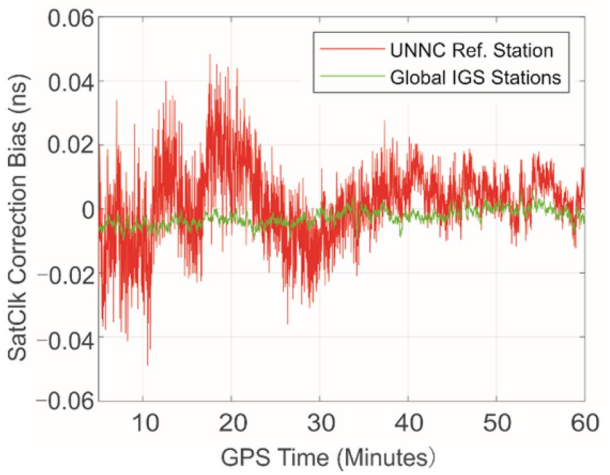


Fig. 5 GPS 03 clock corrections over a 1-h period between 07:00 and 08:00, estimated using the standalone GNSS reference station dataset (red line) and the world-wide distributed IGS reference stations (green line)

$\boldsymbol{u}_i$ is the $m_i \times 32$ matrix coefficient for the satellite clock correction terms, which contains only one "1" and all others coefficients are zeros on each row. The column vector $\boldsymbol{\varphi}_{i,\mathrm{IF}}$ denotes the IF carrier phase measurements of the tracked satellite at the ith station.

The satellite clock correction bias changes at sub-nanosecond level and is illustrated in the top panel of Fig. 4, and cannot be clearly seen in the satellite clock correction plots (for example, PRN16 in Fig. 4 bottom), due to their larger scale variations over a short period. In this case, the satellite clock correction bias is introduced, which is the difference between the estimated satellite clock correction and the linear interpolation time series from the satellite clock product. The top panel of Fig. 4 shows the GPS satellites' clock correction bias. Satellite clock corrections were estimated using the 1 Hz reference stations dataset at UNNC. 13 satellites were tracked over the 4 h period. The gaps in the clock correction time series in the top panel of Fig. 4 are due to the GNSS signal loss at the reference station. The changes in satellite clock correction are no more than ± 0.1 ns, which has a 3 cm influence on the radial range changes for each satellite. The clock correction biases are much larger at the beginning or end of the satellite correction time series in Fig. 4. This is due to the larger errors of satellite carrier phase measurement at low elevations, and the poor observation geometry when a single station is used for the satellite clock estimation. In order to improve the precision of the satellite clock corrections, the IGS stations that are distributed around the world were used for clock correction estimation. Redundant observations improved the estimation. Figure 5 shows the GPS PRN 03 clock correction, estimated using the UNNC

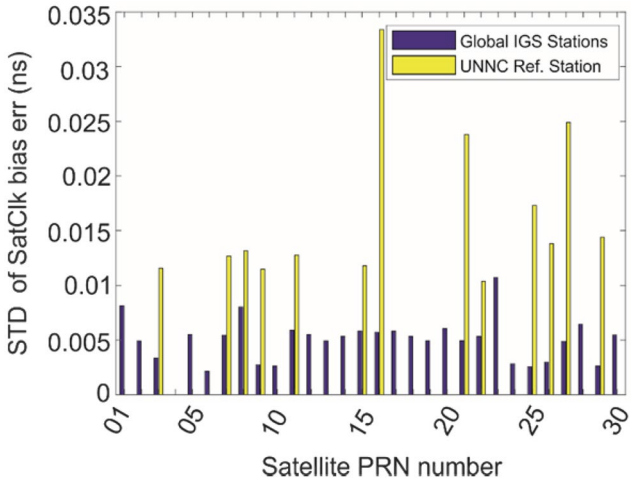


Fig. 6 Standard deviations of GPS satellite clock correction bias, estimated using the UNNC reference station (yellow bar), and global IGS reference stations (blue bar)

reference station dataset and the world-wide distributed IGS stations datasets. This improvement is significant, from $\pm 4 \times 10^{-2}$ ns to $\pm 8 \times 10^{-3}$ ns, with corresponding RMS values of 0.01158 ns and 0.00253 ns respectively. In other words, an improvement from 12 mm to 2.4 mm in the range of the GPS PRN 03 signal.

Figure 6 shows the STD of all satellite clock correction biases which were estimated using the IGS reference stations and the UNNC reference station observations. All STDs of satellite clock correction biases estimated by the global IGS stations are smaller than in the case of the UNNC reference station. This implies the types of error at either the beginning or the end of the satellite clock correction time series (Fig. 4 top) were significantly reduced. The improvement of the satellite clock corrections is due to the better observation geometry of Eq. 8 when the 96 stations are involved. For example, the GPS PRN 16 clock correction bias STD decreases by up to 5.8 times, from 0.0334 ns to 0.0057 ns.

High-rate PPP experiments

The Rotating-arm and Severn Bridge field trials were carried out in order to analyze and assess the high-rate PPP performance for retrieval of the GNSS antenna movement. The rotating-arm is a portable platform that is able to rotate with a constant speed and precise circular motion. Such a controlled experiment means there are fewer uncertainties in the movement time series than in data gathered on a large bridge.

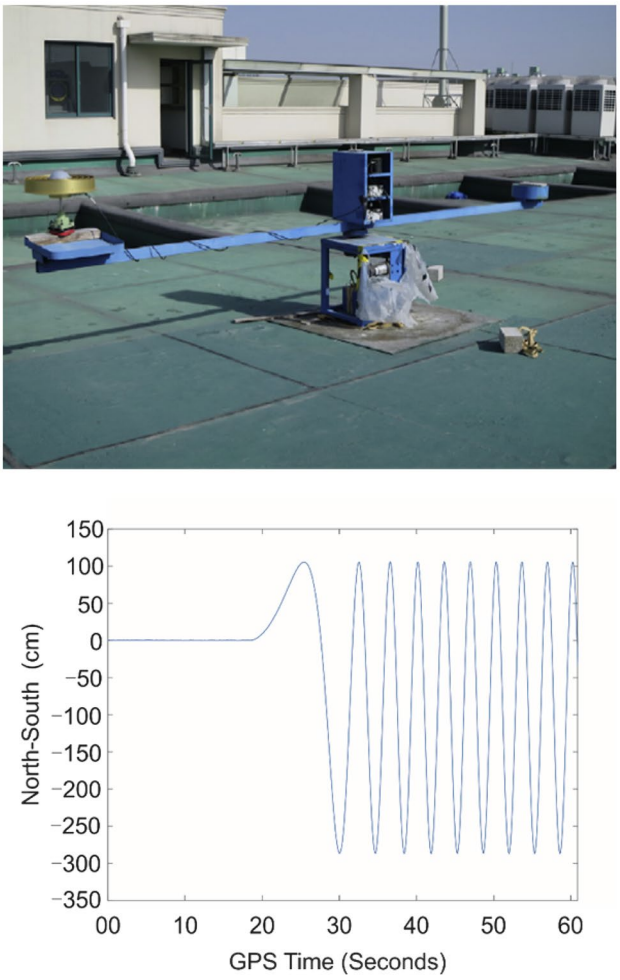


Fig. 7 Rotating-arm apparatus on the roof of SEB at UNNC (top). Antenna North–South component movement (bottom) starting in a static situation to moving at a constant speed over a 60-s period

Rotating-arm rig experiment

The rotating-arm rig was located on the roof of PMB, about 36 meters away from the reference station (Fig. 2 top panel), at UNNC. The arm is about 4 m in diameter. The GNSS antenna was mounted at one end of the bar and counterbalanced with concrete blocks at the other. The antenna used in this experiment was a Leica AR25 choke ring antenna. The receivers and antenna rotate around with the rig, driven by an electric motor. Two Leica GR10 receivers were connected with the antennas at the reference station and the rotating-arm, respectively. All receivers were configured for a sampling rate of 10 Hz and a 10° elevation mask cut off angle was implemented.

The electric motor takes approximately 9 s to reach a constant speed from the static mode. The major movement of the rotating-arm is in the horizontal plane, allowing the North–South and East–West components to be measured.

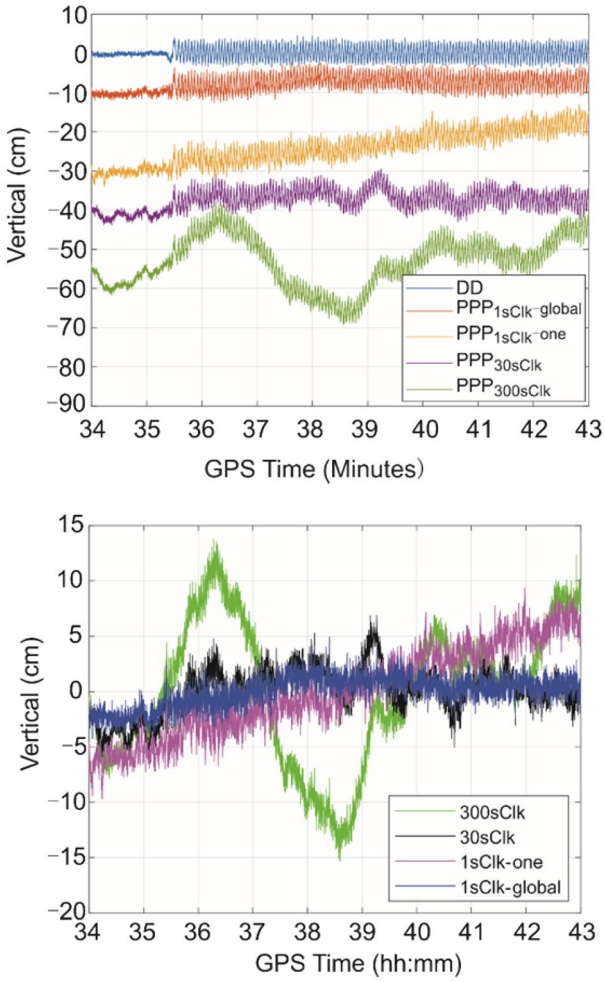


Fig. 8 Rotating-arm antenna vertical movements over a 9-min period between 05:34–05:43, calculated using DD and PPP techniques with different types of satellite clock corrections (top); The vertical differences between DD and each PPP movement time series (bottom)

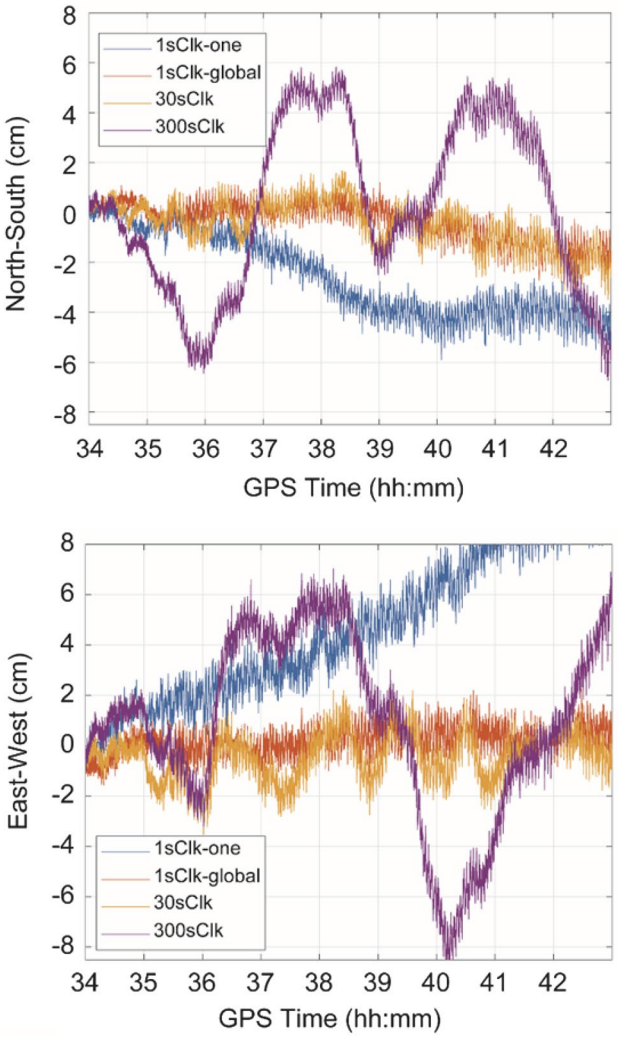


Fig. 9 North–South component (top) and East–West component (bottom) of the differences between the DD and the three PPP results

There are also vertical movements, due to the fact that the rotating-arm is not perfectly horizontal. The top panel of Fig. 7 shows the rotating-arm rig, located in a reasonably open sky environment. The bottom panel of Fig. 7 is the GNSS antenna movement, showing the north–south component over a 1-min period after the electric motor is initially switched on.

The rotating-arm antenna movement was estimated using dynamic PPP with the 1-s interval satellite clock corrections, as well as with the 30- and 300-s interval clock products from the IGS. The DD kinematic method was also used for estimating the rotating-arm movement. The time series of PPP antenna movement was compared against that from DD processing. Figure 8 top panel shows the movement of the rotating-arm in the vertical component. The bottom panel shows the difference between the DD and PPP-derived movements using different types of satellite clock corrections. The 1-s interval satellite clock corrections estimated using the global distributed IGS stations was applied for the PPP processing, and the vertical movements of the antenna agree with the DD results very well, with the root mean square 2.55 cm between DD and PPP results. The PPP results with the satellite clock corrections from the UNNC reference station can be used, but there is an obvious systemic drift. The root mean square between the DD and the PPP results is up to 7.05 cm. This is mainly due to the low precision of the 1-s interval satellite clock corrections estimated by the UNNC standalone reference station. Gradual movement can also be seen in the PPP time series, when either the 30-s interval or 300-s interval satellite clock correction products were applied (Fig. 8). This gradual movement does not appear in the 1 s interval clock PPP results, which suggests that the high-rate precise satellite clock corrections can improve the performance of PPP for

high sampling rate applications. Figure 9 illustrates the differences in the North–South component and the East–West component between the DD-derived results and the three PPP-derived results. Again, these illustrate the improvements in using the 1 s clock corrections, in particular, estimated using data from the global IGS stations.

Severn bridge deflection experiment

The M48 Severn Bridge in the UK is a 1600 m long suspension bridge over the Severn River, connecting Wales and England. The main-span between the two towers is 988 m long. Nine dual-frequency survey-grade GPS/GLONASS receivers were mounted on the bridge, including 4 Leica 1200 dual-frequency receivers and 1 Leica SR510 single-frequency receiver located on the suspending cables, and 4 Leica SR530 dual-frequency receivers located on the supporting towers. Two reference stations located within 2 km of the bridge were established for the DD method. The reference stations were equipped with Leica Viva receivers. The data was collected on two separate occasions, from March 10–12, 2010, and again on March 18, 2010. The data sampling rate was 20 Hz for the Leica 1200 and Leica Viva receivers, and 10 Hz for the Leica SR510 and Leica SR530 receivers. Choke ring antennas were used to reduce the effect of multipath, and a 15° elevation cut-off angle was implemented so as to reduce the random noise at low elevation angles. Only datasets between 15:00 and 18:00 on March 11 were processed in this study, with all stations continually tracking satellites over these 3 h. PPP is sensitive to data gaps as re-convergence is required before a stable position solution can be recomputed.

The Severn Bridge is equipped with anemometers and thermometers, as well as weight in motion (WIM) sensors on the Welsh side of the bridge. These sensors allow analysis of the bridge deflections in conjunction with the temperature and loading changes. The orange points in Fig. 10 show the locations of the GNSS antennas. The WIM sensor is 1522 m away from the support tower at the Beachley side.

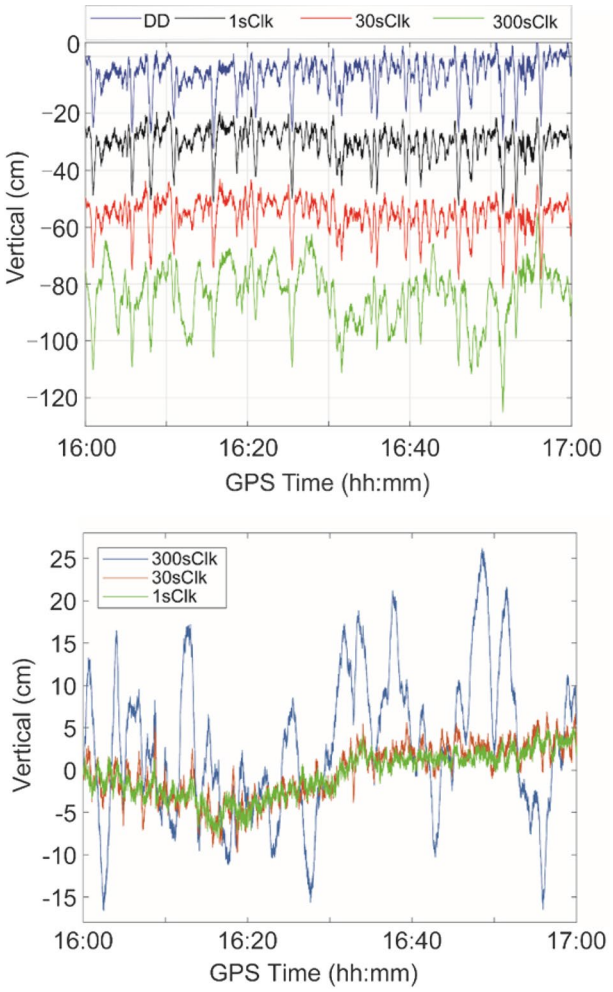


Fig. 11 Bridge deflection vertical component for survey point A over a 1-h period (top). Difference between the three PPP-derived time series and using DD-derived results for the vertical component (bottom)

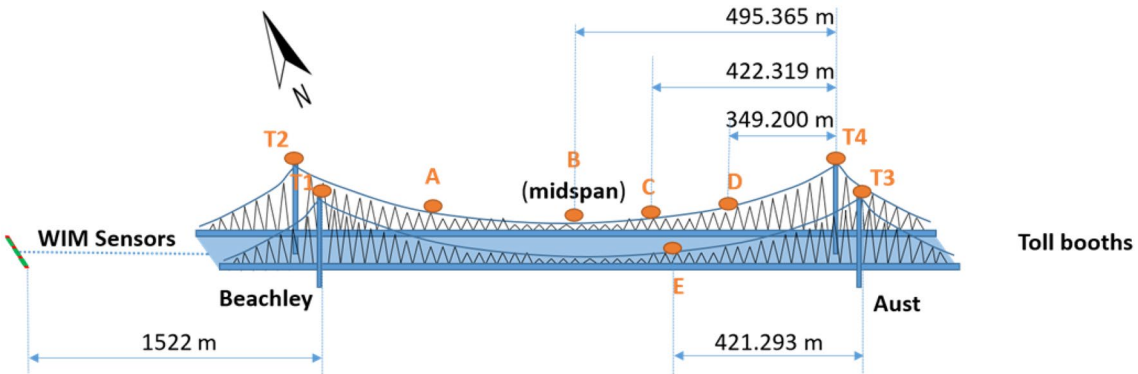


Fig. 10 Survey point locations on the Severn Bridge, UK

The PPP bridge deflection time series, for the vertical component, with the application of 1-s interval satellite clock corrections and IGSACC 30/300-s interval satellite clock corrections are shown in top panel of Fig. 11. The DD-derived time series are treated as the truth and used for assessing the quality of the PPP time series. The differences between the DD time series and the three PPP results are illustrated in Fig. 11 (bottom). The results derived using the 1-s clock corrections in bottom panel of Fig. 11 have the smallest deviation from the DD-derived results. The bridge 20 Hz sampling rate movements are more than 20 cm in the vertical component over a 1 h period. PPP-derived movement time series using 1-s interval and 30-s interval clock corrections agree with the DD results very well. The PPP results using the 300-s interval clock corrections have worse performance than the other three. The correlation coefficient between DD and 300 s interval clock PPP is 0.54. The correlation coefficient between 1 s interval clock PPP and DD results is slightly better than that between 30 s interval PPP and DD, improving from 0.85 to 0.89. These demonstrate that PPP using 1-s interval satellites clocks corrections improves the bridge deflection at the vertical component, comparing with that using 30-s and 300-s interval satellites clocks corrections.

Table 1 shows the correlation coefficient between the PPP time series and DD results at locations A, B, C and D. The improvement of the correlation coefficient is achieved by applying the 1-s interval satellite clock corrections. Only location C's result for the lateral component is slightly worse when using the 1 s interval satellite clocks corrections. The standard deviation of all 4 stations' time series is improved by applying the 1-s interval satellite clocks corrections, except for location D in the lateral component.

Small movements are more difficult to extract from the noisy measurements. The bridge movement of the suspension cable in the vertical component is more than 20 cm, but very small in the longitudinal and lateral components, and small in all three components at the supporting tower. Figures 12 and 13 show the horizontal movements of location A and tower T1, respectively. These figures also illustrate the differences between the DD results and the three sets of PPP results. The 1 s interval clock PPP and 30 s interval clock PPP results agree with the DD results. The 1 s interval clock PPP performance is better than when the 30 s interval clock correction is applied, particularly the portions highlighted as 1, 2, and 3 in Fig. 12. This means that the 1-s interval clock indeed improved the PPP for high sampling rate processing and for small movement detection. The cable movements caused by the bridge oscillating in the longitudinal direction are generally larger than in the lateral direction, which is also reflected in the 1-s interval clock PPP results (see Figs. 12, 13). Figure 13 is the movement time series retrieved at tower T1. The clear waveform in the longitudinal component reflects the movement of the bridge's supporting tower. Figure 12 shows that there were similar gradual movements when both the 1-s interval clock PPP and the PPP with 30-s interval clock correction were applied. This implies there are still some errors that are unmodeled in the 1-s interval clock PPP, for instance, the higher order ionospheric errors and unmodeled ZWD. Figures 11, 12 and 13 illustrate that the 300 s interval clock correction products from IGS are not of sufficient quality for the detection of high-frequency oscillations and small structural movements.

The speed, direction, and weight of vehicles can be recorded by the WIM sensors as the vehicles cross over the bridge. There was no traffic congestion between 16:00 and 17:00 March 11, 2010. With the assumption that each vehicle crosses the bridge at a constant speed, as recorded by WIM sensors, the load of the traffic on the main-span at any

Table 1 Correlation coefficient between high-rate PPP time series and DD. STD of time series for Longitudinal, Lateral and Vertical components

Correlation coefficient												
Survey Point	A			B			C			D		
Sate Clk Int. (second)	1	30	300	1	30	300	1	30	300	1	30	300
Longitudinal	0.67	0.60	0.20	0.53	0.50	0.32	0.55	0.51	0.31	0.58	0.52	0.49
Lateral	0.72	0.67	0.12	0.78	0.77	0.41	0.39	0.41	0.10	0.72	0.71	0.42
Vertical	0.89	0.85	0.54	0.76	0.72	0.47	0.87	0.82	0.51	0.70	0.67	0.38
STD												
Survey Point	A			B			C			D		
Sate Clk Int. (second)	1	30	300	1	30	300	1	30	300	1	30	300
Longitudinal (cm)	1.53	1.90	6.77	3.12	3.56	7.80	3.33	3.81	9.01	1.77	1.98	6.02
Lateral (cm)	1.05	1.27	4.89	2.02	2.19	5.72	2.34	2.50	6.30	2.61	2.59	5.32
Vertical (cm)	2.69	3.14	8.55	5.22	5.85	12.66	3.72	4.52	12.71	5.55	6.18	15.46

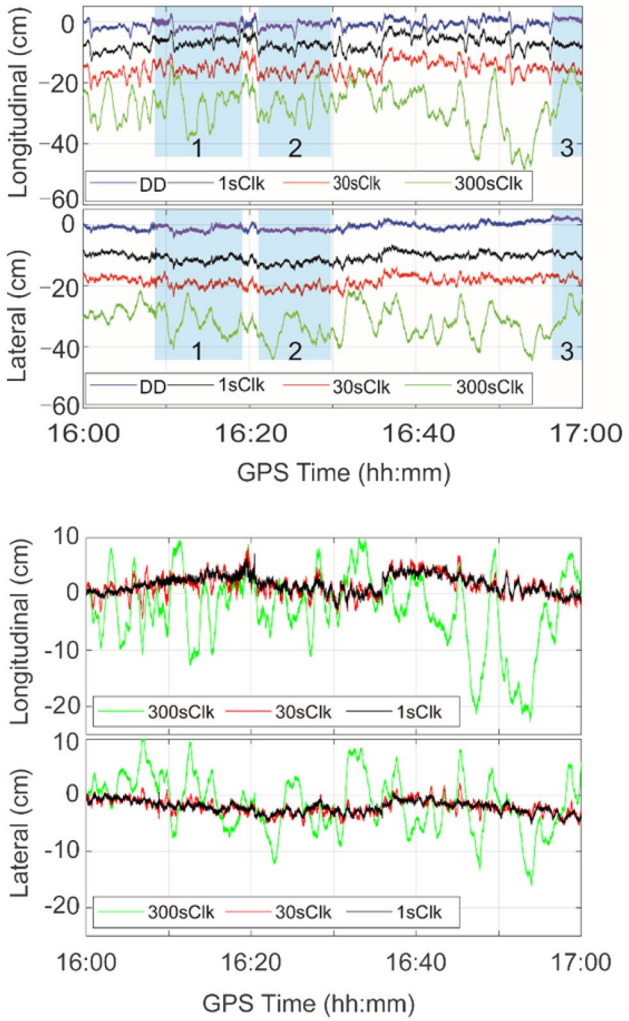


Fig. 12 Lateral and longitudinal deflection time series from DD and PPP processing over 1-h period at location A (top). Differences between the three PPP time series and that of DD at location A (bottom)

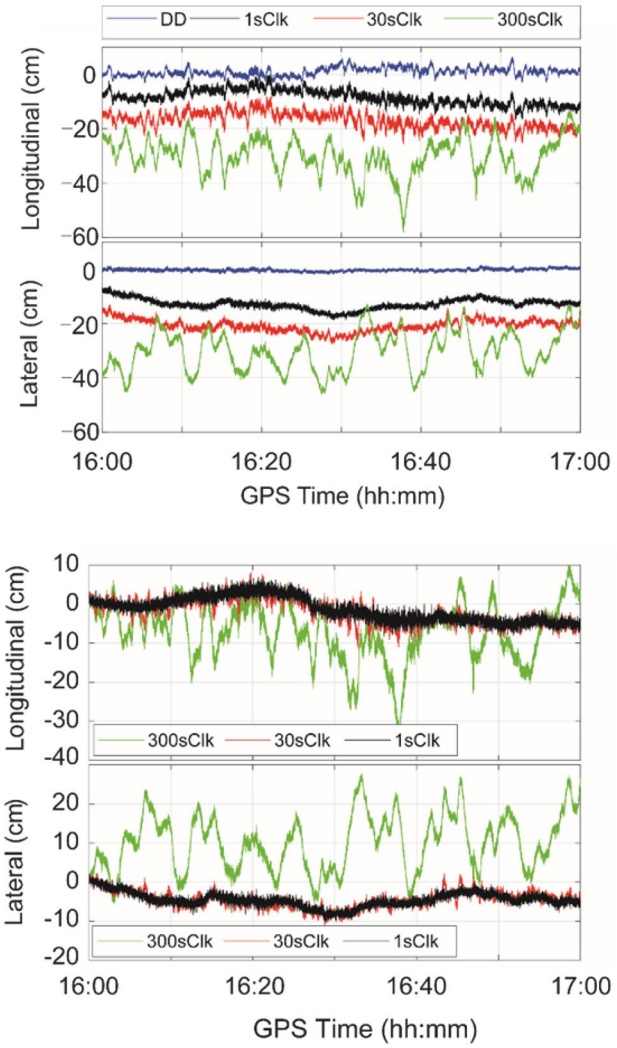


Fig. 13 Lateral and longitudinal deflection time series from DD and PPP processing over 1-h period at location T1 (top). Differences between the three PPP time series and that of DD at location T1 (bottom)

instant can be estimated. Figure 14 shows the four cables and four tower surveying point time series for the vertical and longitudinal components. The consistency of the WIM time series compared with the bridge cable surveying point movements implies that the bridge movements are largely due to the traffic loading (Fig. 14). Location A, B and C are on the north-side of the bridge's main-span, Location E is on the south-side of bridge main-span. Figure 14 demonstrates that both sides of the main-span have synchronous deflections while either north-side or south-side of bridge has big weight loadings. The corresponding movements at the tower surveying point in the longitudinal component indicate that 1-s interval clock PPP is able to monitor the movements of large structures, such as a long bridge, with high-frequency, small oscillating movements.

Conclusion

We investigated the use of kinematic PPP technique for bridge deflection measurement, with the aid of 1-s interval satellite clock correction. The procedure for 1 Hz satellite clock correction estimation was explained in detail. A standalone reference station dataset was first used for estimating the satellite clock corrections, in addition 96 globally distributed IGS reference stations were used to estimate the clock corrections. The results reveal the improvement of the estimated satellite clock corrections when using a large number of reference stations compared to using data from single station. Using a rotating-arm apparatus, an experiment with constant rotating speed was carried out. The results showed that the PPP performance was improved by applying the

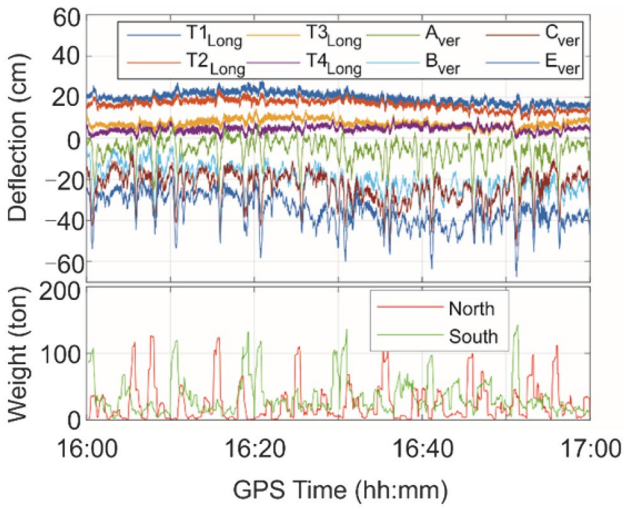


Fig. 14 1 s interval satellite clock PPP movement comparison of cable and tower surveying points (top panel). Bridge weight loading on the north-side highway and the south side highway (bottom panel)

high-rate satellite clock corrections estimated using the 96 IGS stations dataset compared to using IGSACC 30 s or 300 s satellite clock products. Validation of the method was also carried out using a real-world dataset from the long-span Severn Bridge, UK. The bridge experiment shows the PPP with high-rate satellite clock corrections can detect small movements, which is not possible when using the 300 s satellite clock products from the IGS. PPP offers an alternative approach for precise structural deflection monitoring when the DD method cannot be used, but there are still some points that need to be addressed. PPP can only give precise deflection after a few minutes of convergence time, re-initialization is also required after the signal is interrupted. Current development of multi-GNSS PPP can help to solve these issues.

Acknowledgements The authors acknowledge the IGS for providing the high-rate GPS observations, satellite clock and orbital products. Authors are grateful to the anonymous reviewers, whose comments significantly improved this manuscript. This work is supported by the Young Scientist program of the Natural Science Foundation of China (NSFC) with a project code 41704024; another 2 general programs of NSFC with project codes No.41774034 and No. 41774030 and NSFC key project with No. 41830110; the Zhejiang Provincial Natural Science Foundation of China under Grant No. LY16D040001, as well as Ningbo Science and Technology Bureau—China as part of the project Structural Health Monitoring of Infrastructure in the Logistics Cycle (2014A35008).

References

Ashkenazi V, Roberts GW (1997) Experimental monitoring of the humber bridge using GPS. Proc Inst Civ Eng 120(4):177–182

Bock H, Dach R, Jäggi A, Beutler G (2009) High-rate GPS clock corrections from CODE: support of 1 Hz applications. J Geod 83(11):1083–1094. https://doi.org/10.1007/s00190-009-0326-1

Feng Y, Gu S, Shi C, Rizos C (2013) A reference station-based GNSS computing mode to support unified precise point positioning and real-time kinematic services. J Geod 87(10–12):945–960. https://doi.org/10.1007/s00190-013-0659-7

Kaloop MR, Li H (2009) Monitoring of bridge deformation using GPS technique KSCE. J Civ Eng 13(6):423–431. https://doi.org/10.1007/s12205-009-0423-y

Liu Y, Ye S, Song W, Lou Y, Chen D (2017) Integrating GPS and BDS to shorten the initialization time for ambiguity-fixed PPP. GPS Solut 21(2):333–343. https://doi.org/10.1007/s10291-016-0525-1

Moschas F, Avallone A, Saltogianni V, Stiros SC (2014) Strong motion displacement waveforms using 10-Hz precise point positioning GPS: an assessment based on free oscillation experiments. Earthq Eng Struct Dyn 43(12):1853–1866. https://doi.org/10.1002/eqe.2426

Msaewe HA, Hancock CM, Psimoulis PA, Roberts GW, Bonenberg L, de Ligt H (2017) Investigating multi-GNSS performance in the UK and China based on a zero-baseline measurement approach. Measurement 102:186–199. https://doi.org/10.1016/j.measurement.2017.02.004

Niell AE (1996) Global mapping functions for the atmosphere delay at radio wavelengths. J Geophys Res 101(B2):3227–3246 DOI. https://doi.org/10.1029/95jb03048

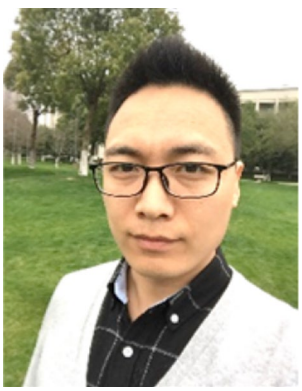
Roberts GW, Brown CJ, Tang X, Meng X, Ogundipe O (2014) A tale of five bridges; the use of GNSS for monitoring the deflections of bridges. J Appl Geod 8(4):241–264. https://doi.org/10.1515/jag-2014-0013

Tang X, Li X (2017a) Differenced measurements between satellites applied on RTK PPP for structure monitoring. In: J. Sun et al. (eds), China satellite navigation conference (CSNC) 2017. Proceedings: Volume 1, lecture notes in electrical engineering 437: 277–284, May 23–25, Shanghai, China. https://doi.org/10.1007/978-981-10-4588-2_24

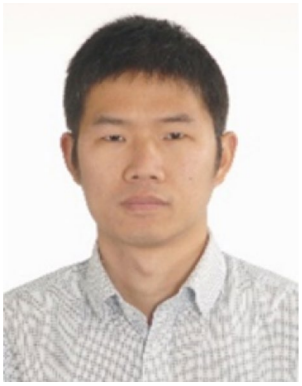
Tang X, Roberts GW, Li X, Hancock CM (2017b) Real-time kinematic PPP GPS for structure monitoring applied on the severn suspension bridge, UK. Adv Space Res 60(5):925–937. https://doi.org/10.1016/j.asr.2017.05.010

Yi TH, Li HN, Gu M (2013) Experimental assessment of high-rate GPS receivers for deformation monitoring of bridge. Measurement 46(1):420–432. https://doi.org/10.1016/j.measurement.2012.07.018

Publisher's Note Springer Nature remains neutral with regard to jurisdictional claims in published maps and institutional affiliations.



Xu Tang is a research fellow in the department of Civil Engineering at the University of Nottingham Ningbo China. He obtained his BSc and Ph.D. degree from Nanjing Forestry University and Hohai University, respectively, in 2008 and 2014. His research interest covers various aspects of Engineering Surveying, Deformation Monitoring, GNSS Clock Estimation, research into GNSS PPP for Structure Deflection Detection, Vapor Remote Sensing using GNSS, etc.



Xingxing Li is a professor at Wuhan University. He received his BSc and Ph.D. degrees with distinctions in Survey Engineering and Geodesy from Wuhan University in 2008 and 2013, respectively. His current research mainly involves GNSS precise positioning and orbit determination and its application for geosciences.



Gethin Wyn Roberts is an Associate Professor at Fróðskaparsetur (University of the Faroe Islands). He has authored and coauthored over 200 papers, co-supervised 25 Ph.D. students and been the investigator on UK and international research grants. He is past Chairman of the FIG's Commission 6, Engineering Surveys, and previously held posts at the University of Nottingham both in the UK and in China. He is a recipient of the Zhejiang Province 1000 Talent programme and Fellow of the Chartered Institution of Civil Engineering Surveyors, and a Fellow of the Higher Education Academy. He holds a 1st class honors degree BEng in Mining Engineering and a Ph.D. in Engineering Surveying and Geodesy both from the University of Nottingham, UK.



Craig Matthew Hancock is currently Head of Civil Engineering at the University of Nottingham Ningbo China campus. He obtained a degree in surveying and mapping science from Newcastle University (UK) and a Ph.D. in Space Geodesy also from Newcastle University (UK). His main research interests are GNSS Ionospheric error mitigation and Structural Monitoring.



Huib Ligt is a teacher at the University of Nottingham in Ningbo China in all the practical aspects of engineering surveying and geodesy. He obtained his MSc degree in geodetic engineering from the Delft University of Technology in the Netherlands. After working at the University of Nottingham in the UK for five years as an experimental officer, Huib worked two years at Septentrio Satellite Navigation in Belgium as a test automation engineer.



Fei Guo is currently an Associate Professor at the school of Geodesy and Geomatics, Wuhan University, China. He received his BSc degree in Survey Engineering from Nanjing Forestry University in 2007. He obtained his MSc and Ph.D. degrees with distinction in Geodesy from Wuhan University in 2009 and 2013, respectively. His current research mainly focuses on GNSS-related quality assessment, quality control, and precise point positioning.